

Article

Theoretical Study on the Structures, Electronic Properties, and Aromaticity of Thiophene Analogues of Anti-Kekulene

Shingo Hashimoto and Kazukuni Tahara *

Department of Applied Chemistry, School of Science and Technology, Meiji University, 1-1-1 Higashimita, Tama-ku, Kawasaki 214-8571, Kanagawa, Japan

* Correspondence: tahara@meiji.ac.jp; Tel.: +81-(044)-934-7213

Abstract: We predict the geometries, electronic properties, and aromaticity of thiophene analogues of anti-kekulene with six to nine thiophene rings **1–4**, together with those of cyclobutadithiophenes (CDTs) and anti-kekulene as reference compounds, using density functional theory calculations. Investigation of the simplest reference compounds, CDTs, reveals that the local aromaticity of their thiophene rings is influenced by their fused position (*b*- or *c*-bond) to the four-membered ring (4MR). A thiophene ring fused at the *b*-position (*b*-TR) retains its aromatic character to some extent, whereas the aromatic character of one fused at the *c*-position is attenuated. The 4MR with two fused *b*-TRs retains a strong anti-aromatic character. Thiophene analogues of anti-kekulene with six to eight thiophene rings **1–3** favor bowl-shaped structures, in contrast to the planar structure of anti-kekulene, because of the shorter distances of the sulfur bridges. Compound **4**, with nine thiophene rings, adopts a planar structure. The local aromaticity and anti-aromaticity of the thiophene ring and 4MR are significantly attenuated in **1–4** compared with the reference compounds, the CDTs and anti-kekulene. This can be attributed to the considerable contribution of the quinoidal electronic structure in **1–4**. The present study provides new insight into the aromatic and electronic nature of systems containing cyclobutadienothiophene.



Citation: Hashimoto, S.; Tahara, K. Theoretical Study on the Structures, Electronic Properties, and Aromaticity of Thiophene Analogues of Anti-Kekulene. *Chemistry* **2022**, *4*, 1546–1560. <https://doi.org/10.3390/chemistry4040102>

Academic Editor: Ryan C. Fortenberry

Received: 27 September 2022

Accepted: 8 November 2022

Published: 11 November 2022

Publisher's Note: MDPI stays neutral with regard to jurisdictional claims in published maps and institutional affiliations.



Copyright: © 2022 by the authors. Licensee MDPI, Basel, Switzerland. This article is an open access article distributed under the terms and conditions of the Creative Commons Attribution (CC BY) license (<https://creativecommons.org/licenses/by/4.0/>).

Keywords: polycyclic aromatic compounds; aromaticity and anti-aromaticity; cyclobutadiene; anti-kekulene; quinoidal electronic structure; macrocycles; DFT calculation

1. Introduction

Polycyclic compounds consisting of aromatic and anti-aromatic rings are a subject of interest because of their unique optical and electronic properties that originate from modulated (anti-)aromaticity [1–8]. Examples of these compounds include biphenylene (Figure 1a), which consists of two benzene rings and a four-membered ring (4MR) [9,10]. Extended analogues of biphenylene, known as [n]phenylenes, are composed of n-numbered benzene rings and 4MRs in an alternating manner [11]. Vollhardt and different co-authors have studied the syntheses and properties of [n]phenylenes of various sizes and topologies (e.g., linear [12], angular [13], and branched [14]; Figure 1b). The influence of topological differences on the aromaticity and electronic properties of these compounds has been studied using both experimental and theoretical approaches [11,15–21]. Anti-kekulene (cyclic [6]phenylene) has been a subject of particular interest because of its unique structure, electronic properties, and aromaticity, as predicted by quantum chemical calculations (Figure 1c) [19–27]. For instance, density functional theory (DFT) calculations predicted that anti-kekulene favors a planar structure with strong bond length alternation in fused benzene rings [19,21,25]. Moreover, Hückel–London–Pople–McWeeny (HLPM) topological ring-current and bond-current calculations [28,29], which are simple approaches to ring current calculation based on Hückel–London formalism [30,31], have confirmed both paratropic ring current flows at 4MRs and an outer periphery featuring an overall weakly paratropic character [24]. Despite several efforts using different synthetic approaches, the synthesis of anti-kekulene has not yet been achieved [32–34].

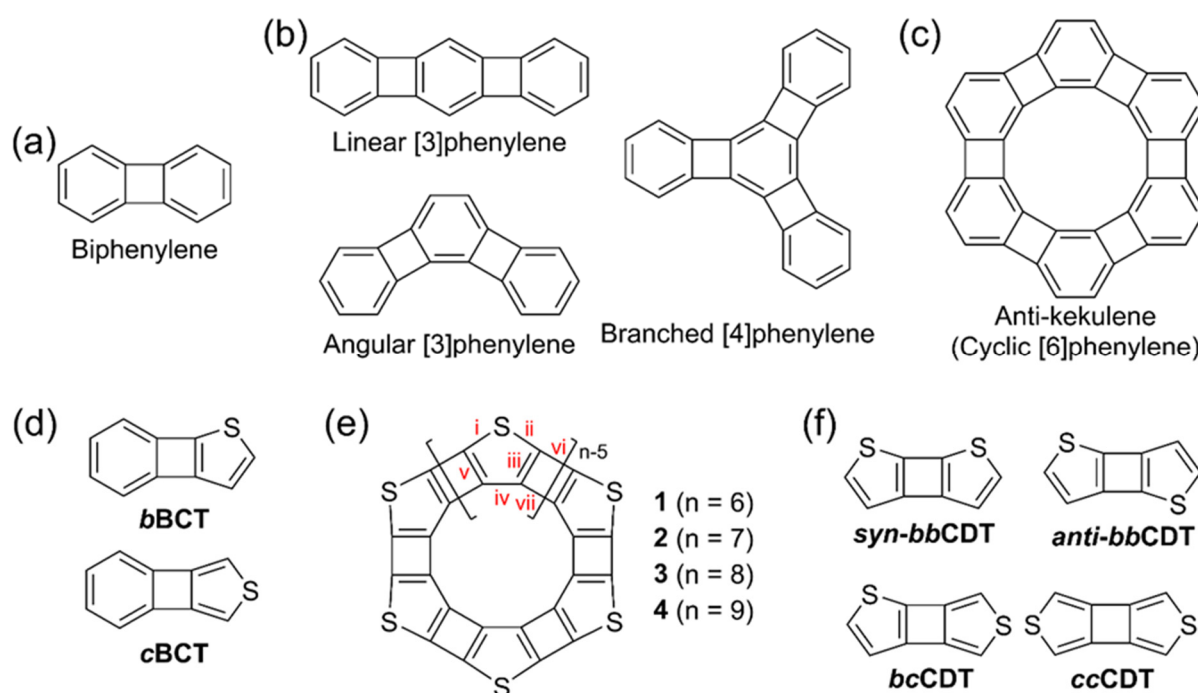


Figure 1. Chemical structures of (a) biphenylene; (b) [n]phenylenes of different sizes and topologies: linear [3]phenylene, angular [3]phenylene, and branched [4]phenylene; (c) anti-kekulene (cyclic [6]phenylene); (d) *b*BCT and *c*BCT; (e) thiophene analogues of cyclic [n]phenylenes 1–4; and (f) four CDTs, *syn-bb*CDT, *anti-bb*CDT, *bc*CDT, and *cc*CDT. In (e), Roman numerals (i–vii) on 1–4 indicate bond positions.

Annulation of thiophene ring(s) into polycyclic compounds is a useful way to produce functional organic materials as it influences fundamental properties including molecular geometry, electronic configuration, and aromaticity. Moreover, it modulates optoelectronic properties and intermolecular interaction modes [35–41]. For instance, octathia [8]circulene (sulflower) [42], in which eight benzene rings of a saddle-shaped [8]circulene [43,44] are fully replaced with thiophene rings, has a planar structure [45]. Its one-dimensional π -stacking column with short intermolecular sulfur–sulfur contacts in the crystalline state exhibits a reasonable field-effect transistor property [46,47]. Moreover, some thiophene-fused acene derivatives [35,48] are promising organic semiconductors because of their stability and high mobility. The annulation of thiophene ring(s) into an (anti-)aromatic ring also has a strong impact on electronic properties and on local and global aromaticity [49–52]. The fusion position, i.e., the *b*- or *c*-position of the thiophene ring, determines such properties because of the diene character of thiophene [53,54]. For instance, the aromaticity of dehydro[14]annulene derivatives with a fused thiophene ring at the *b*-position (*b*-TR) is stronger than that of isomers with one fused thiophene ring at the *c*-position (*c*-TR) [55,56]. Similar observations have been reported for other dehydrothiophenoannulene derivatives with two to three fused thiophene rings [57,58]. Moreover, we recently reported that the attenuation of the anti-aromaticity of 12-membered rings is limited for those with two or three *b*-TRs, but significant for the *c*-isomers [59]. The same tendency has been reported for 8π electron systems, such as thienopentalene derivatives [60,61]. This change in aromaticity leads to modulation of the molecular orbital energies.

The substitution of the benzene ring(s) of biphenylene and [n]phenylene with thiophene ring(s) has a similar impact on aromaticity and electronic properties. Benzo[3,4]cyclobuta[1,2-*c*]thiophene (*c*BCT; Figure 1d) [62,63] and its regioisomer benzo[3,4]cyclobuta[1,2-*b*]thiophene (*b*BCT) [64], both synthesized over 40 years ago, have been reported to differ in stability in an ambient environment; *c*BCT is persistent, whereas *b*BCT decomposes within a few hours. We recently performed quantum chemical calculations for BCTs at

the DFT level to investigate their geometries, electronic properties, and aromaticity [65]. The anti-aromaticity of the 4MR of the *b*-isomer was greater than that of the *c*-isomer, and the energy gap (E_{gap}) between the highest occupied molecular orbital (HOMO) and the lowest unoccupied molecular orbital (LUMO) was small for the *b*-isomer. We extended the study of these compounds to their homologues, in which the terminal benzene rings of [n]phenylenes are replaced by thiophene rings. The aromaticity and electronic properties of these extended homologues also differed depending on the fused position of the thiophene rings. As this previous investigation was limited to its substrate scope, further studies of the extended systems containing cyclobutathiophene moieties are required for an in-depth understanding of the systems and their novel molecular design. Cyclic systems are of particular interest because of their ability to form macrocyclic π -conjugation pathways.

In this context, we herein report a theoretical study on the thiophene analogues of cyclic [n]phenylenes 1–4, where all thiophene rings are fused to 4MRs at the *b*-position, in which we investigate their geometries and aromaticity based on DFT calculations (Figure 1e). Together with 1–4, as reference compounds we investigated the geometries and aromaticity of four cyclobutadithiophenes (CDTs; Figure 1f) [66,67], cyclobuta[1,2-*b*:4,3-*b'*]dithiophene (*syn-bb*CDT) and its regioisomer (*anti-bb*CDT), cyclobuta[1,2-*b*:3,4-*c'*]dithiophene (*bc*CDT), and cyclobuta[1,2-*c*:3,4-*c'*]dithiophene (*cc*CDT), as well as anti-kekulene. In *syn-bb*CDT, which is the simplest substructure of 1–4, the aromaticity and anti-aromaticity of the TRs and 4MR were preserved. On the other hand, local aromaticity and anti-aromaticity were significantly attenuated for the thiophene analogues of cyclic [n]phenylenes 1–4 because of the major contributions of the quinoidal electronic structure [68,69]. The results of the present study will be useful for the further design of novel polycyclic compounds containing thiophene rings and 4MRs.

2. Materials and Methods

All quantum chemical calculations were performed using the Gaussian 16 program package under vacuum (revision A.03) [70]. All molecular geometries were optimized at the B3LYP/6-311+G(d, p) level of theory with Grimme's dispersion correction method D3 [71] and Becke–Johnson damping (D3BJ) [72] in the closed-shell singlet state. Vibrational frequency calculations confirmed the absence of imaginary frequencies for all optimized geometries. The convergence criteria in all geometry optimizations (maximum force, root mean square (RMS) force, maximum displacement, and RMS displacement) were set to 5×10^{-4} a.u. We confirmed that this level of theory reliably reproduces a single-crystal X-ray structure of the related molecule, biphenylene [73], confirming the validity of the selection of this functional theory (bond length differences are within 0.01 Å). The closed-shell wavefunctions at optimized geometries were confirmed to be stable [74]. Molecular orbitals and structures were visualized using the Gauss View (version 6.0.16) [75] and Visual Molecular Dynamics (VMD) programs (version 1.9.3) [76].

To analyze the planarity of the compounds quantitatively, we calculated the molecular planarity parameter (MPP) proposed by Lu [77]. This is a simple and universal method to determine molecular planarity based on the deviation of given atoms from a fitting plane determined by the coordinates of all atoms. The fitting planes were calculated using the least squares method. The MPP values were obtained using Equation (1):

$$\text{MPP} = \sqrt{\frac{1}{N} \sum_i d_i^2} \quad (1)$$

where N is the total number of atoms and d_i is the distance between atom i and the fitting plane. The MPP value of a planar molecule is zero; it becomes larger for a non-planar molecule. Moreover, we obtained colored maps of molecular structures according to the d_i value of each atom using the VMD program (Figures S1 and S2). The MPP calculations were performed using the Multiwfn program (version 3.8) [78].

For the quantitative evaluation of the strain in **1–3**, we calculated the relative strain energies (E_{strain}) with respect to nearly planar **4** using a method proposed by Nenajdenko et al. (Table S1) [42].

We employed a harmonic oscillator model of aromaticity (HOMA) analysis as the structural criterion for the local aromaticity and non-aromaticity of the benzene and thiophene rings [79,80]. The HOMA values of the benzene rings were calculated using Equation (2) with individual bond lengths R_i :

$$\text{HOMA} = 1 - \frac{\alpha_{\text{CC}}}{6} \sum_i^6 (R_{\text{opt,CC}} - R_{\text{CC},i})^2 \quad (2)$$

whereas the HOMA values of the thiophene rings were calculated using Equation (3):

$$\text{HOMA} = 1 - \left\{ \frac{\alpha_{\text{CC}}}{3} \sum_i^3 (R_{\text{opt,CC}} - R_{\text{CC},i})^2 + \frac{\alpha_{\text{CS}}}{2} \sum_i^2 (R_{\text{opt,CS}} - R_{\text{CS},i})^2 \right\} \quad (3)$$

where the subscripts CC and CS denote carbon–carbon and carbon–sulfur bonds, respectively. The optimal bond lengths R_{opt} and constants α were derived from Equations (4) and (5), respectively:

$$R_{\text{opt},j} = (R_{s,j} + wR_{d,j}) / (1 + w) \quad (4)$$

$$\alpha_j = 2 \left[(R_{s,j} - R_{\text{opt},j})^2 + (R_{d,j} - R_{\text{opt},j})^2 \right]^{-1} \quad (5)$$

In these equations, the subscript j denotes the bond type (CC or CS, not single or double bond); R_s and R_d correspond to the reference lengths for single and double bonds, respectively; and w is the ratio of force constants for double and single bonds. The values of R_{opt} and α were obtained from the literature [80]. HOMA values close to 1 indicate a high degree of cyclic π -electron delocalization, and smaller values indicate poor π -electron delocalization. The HOMA values were calculated using the Multiwfn program [78].

The multicenter bond index (MCI) is a widely used aromaticity descriptor calculated on the basis of electron delocalization [81,82]. The MCI of a ring consisting of atoms A, B, C, ..., K can be obtained using Equation (6):

$$\text{MCI} = \sum_{\alpha \in A} \sum_{\beta \in B} \sum_{\gamma \in C} \cdots \sum_{\kappa \in K} (PS)_{\alpha\beta} (PS)_{\beta\gamma} (PS)_{\gamma\delta} \cdots (PS)_{\kappa\alpha} \quad (6)$$

In this equation, the Greek subscripts $\alpha, \beta, \gamma, \dots, \kappa$ are the basis functions, and summations extend only over the range of the basis functions centered on a certain atom A, B, C, ..., K. The parameters P and S are the charge bond order and overlap matrix, respectively. Density matrices in the natural atomic orbitals [83] were computed using the NBO 3.1 program implemented in the Gaussian 16 program [84]. The MCI values were calculated using the Multiwfn program [78]. A large MCI value indicates strong aromaticity at the ring, whereas a small MCI value indicates non-aromaticity at the ring.

In order to characterize bonding nature, the Wiberg bond indices (WBI) [85] on the basis of natural atomic orbitals [83] were calculated using the NBO 3.1 program implemented in the Gaussian 16 program [84]. Moreover, a localized orbital locator (LOL) analysis [86,87] was performed using the Multiwfn program [78]. The LOL analysis was useful for the visualization of the behavior of electron (de)localization. In this study, only the contribution of π -type molecular orbitals was considered in the LOL analysis (LOL- π). The calculated LOL- π isosurfaces were visualized using the VMD program [76]. The MCI, WBI, and LOL- π analyses were performed at the B3LYP-D3BJ/6-311G(d, p) level of theory.

Nucleus-independent chemical shift (NICS) values provide a convenient and useful measure of the degree of local ring current effects in π -conjugated systems [88]. In this study, we used NICS(1) $_{zz}$, which is the zz component of the isotropic NICS value calculated at 1 Å above the ring centers (NICS(1) $_{\text{iso}}$) [89]. In the case of the bowl-shaped molecules,

the NICS(1)_{zz} values calculated on the convex face of the molecular bowls were used in discussions. The NICS(1)_{zz} values of the concave face are summarized in Table S3. The coordinates of the ghost atom (Bq) and the NICS(1)_{zz} value were calculated using the Multiwfn program [78]. In an aromatic ring, the external magnetic field induces a diatropic ring current, leading to magnetic shielding at the ring, which results in a negative NICS value. Conversely, in an anti-aromatic ring, a paratropic ring current is induced, resulting in deshielding at the ring, which results in a positive NICS value. In a non-aromatic ring, the absolute value is close to zero. It should be noted that NICS(1)_{zz} analysis gives more reliable results for magnetic response compared with NICS(1)_{iso} or NICS(0)_{iso} in the case of a planar system [89]. The magnetically induced current (MIC) strengths and the current densities were calculated using the gauge-including magnetically induced current (GIMIC, version 2.1.4) method [90,91]. This has been extensively used and is known to give results comparable to those of the graph-theoretical [28,29,92–94] and the continuous transformation of the origin of the current density (CTOCD) approaches [95,96]. Prior to the GIMIC calculations, information about atomic orbital density matrices, first-order perturbed atomic orbital density matrices, molecular coordinates, and basis functions were obtained from the magnetic shielding calculations. The input files for the GIMIC program were generated using the Gaussian2gimic.py program [97]. Each current strength was calculated by numerical integration of the MIC density flowing across a plane perpendicularly to the molecular plane and bisecting the chosen chemical bond. The current paths are represented by arrows. The clockwise and counterclockwise current flows indicate diatropic and paratropic ring currents, respectively. The current strength is given in nA/T. For example, benzene exhibits diatropic and paratropic currents of 16.9 nA/T and 5.1 nA/T, respectively. In total, a diatropic current of 12 nA/T flows in a clockwise manner (Figure S3). Thiophene shows a clockwise diatropic current of 11 nA/T in total. On the other hand, cyclobutadiene shows a counterclockwise paratropic current of 20 nA/T. The signed modulus of the current densities (Figures S8–S10) were visualized using the ParaView program (version 5.8.1) [98]. The grid information for the calculations of current density was obtained using the Multiwfn program [73]. All magnetic shielding calculations were conducted at the B3LYP/6-311+G(d, p) level of theory employing the gauge-independent atomic orbital (GIAO) method [31].

3. Results and Discussion

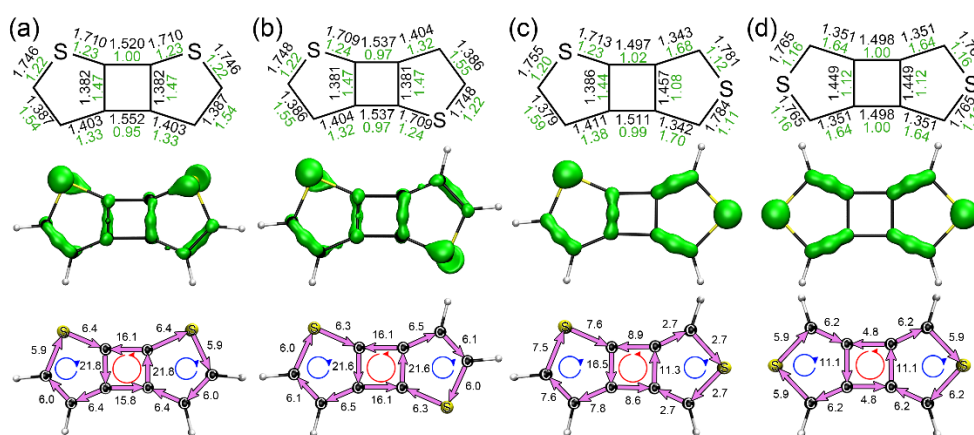
3.1. Structures, Electronic Properties, and Aromaticity of Cyclobutadithiophenes

First, we discuss the structures, aromaticity, and electronic properties of the four CDTs as the simplest models of cyclic systems 1–4.

The geometry optimizations of *syn*- and *anti-bb*CDTs afforded non-planar C₂ and C_i symmetric structures with MPP values of 0.070 Å and 0.066 Å, respectively (Table 1 and Figure S1). On the other hand, the geometry optimizations of *bc*CDT and *cc*CDT gave planar structures with C_s and C_{2h} symmetry groups. There were very small differences in the bond lengths (bond orders), aromaticity, zero-point-corrected total energy, and frontier orbital energy levels of the *bb*CDTs. The lengths and WBI values of the fused bonds of the *bb*CDTs were 1.38 Å and 1.47, respectively, indicating a double bond character (Figure 2a,b). The lengths of the fused bonds differed in *bc*CDT depending on the fused position of the thiophene ring (Figure 2c). Accordingly, the WBI value of the fused bond of the *b*-TR was larger than that of the *c*-TR. In the case of *cc*CDT, the lengths and WBI values of the fused bonds were 1.449 Å and 1.12, indicating a single bond character (Figure 2d). For the non-shared bonds of the CDTs, the *b*-bonds in both *b*- and *c*-TRs had a double bond character (WBI values of 1.54–1.70), whereas the *c*-bonds in the *b*-TRs showed an intermediate character with WBI values of 1.32–1.33. The bonding character of the fused thiophene rings was in agreement with the findings of our previous study on thiopheno[12]annulenes [59]. All bridging bonds in the 4MRs exhibited a single bond character. The LOL- π analyses of the CDTs also supported larger π -electron densities at the *b*-bonds in all thiophene rings (Figure 2).

Table 1. HOMA, MCI, and NICS(1)_{zz} values for 1–4 and reference compounds *syn-bb*CDT, *anti-bb*CDT, *bc*CDT, *cc*CDT, and anti-kekulene.

Compound	HOMA Value			MCI Value				NICS(1) _{zz} Value (ppm)			
	Thiophene Ring		Benzene Ring	Thiophene Ring		Benzene Ring	4MR	Thiophene Ring		Benzene Ring	Macrocyclic Center
	<i>b</i> -TR	<i>c</i> -TR		<i>b</i> -TR	<i>c</i> -TR			<i>b</i> -TR	<i>c</i> -TR		
<i>syn-bb</i> CDT (C ₂) ^a	0.875	—	—	0.0758	—	—	52.5	−16.3	—	—	—
<i>anti-bb</i> CDT (C _i) ^a	0.870	—	—	0.0766	—	—	53.0	−16.4	—	—	—
<i>bc</i> CDT (C _s) ^a	0.831	0.126	—	0.0685	0.0401	—	29.2	−19.1	−5.2	—	—
<i>cc</i> CDT (D _{2h}) ^a	—	0.373	—	—	0.0514	—	17.8	—	−14.3	—	—
anti-kekulene (D _{6h}) ^a	—	—	0.448	—	—	0.0484	24.3	—	—	1.9	16.6
1 (C _{6v}) ^a	−0.707	—	—	0.0121	—	—	8.9	−0.9	—	—	5.7
2 (C _{7v}) ^a	−0.683	—	—	0.0121	—	—	10.7	−0.9	—	—	4.7
3 (C ₈) ^a	−0.661	—	—	0.0128	—	—	10.9	−0.8	—	—	4.9
4 (D ₉) ^a	−0.643	—	—	0.0129	—	—	11.6	−0.5	—	—	4.3

^a Symmetry group of the optimized geometries in parentheses.**Figure 2.** Bond lengths (black numbers, top), WBI values (green numbers, top), LOL- π isosurfaces (isovalue of 0.60 a.u., middle), and paths and strengths (nA/T) of MICs (bottom) for each bond of *syn-bb*CDT (a), *anti-bb*CDT (b), *bc*CDT (c), and *cc*CDT (d).

Next, we investigated the local aromaticity of the CDTs using structural (HOMA), electronic (MCI), and magnetic (NICS and GIMIC) criteria. As additional references, benzene, thiophene, and cyclobutadiene were also subjected to these analyses (Figure S3 and Table S2). The HOMA values for the *b*-TRs of *syn-bb*CDT, *anti-bb*CDT, and *bc*CDT were larger than that of thiophene (Tables 1 and S2). On the other hand, those of the *c*-TRs in *bc*CDT and *cc*CDT were very small. The MCI values of the *b*-TRs were larger than those of the *c*-TRs (Table 1), whereas they were comparable to that of thiophene. This indicates that cyclic conjugation is preserved in the *b*-TR. The NICS(1)_{zz} values of the *b*-TRs in *syn-bb*CDT, *anti-bb*CDT, and *bc*CDT were larger than that of thiophene (Tables 1 and S2). The NICS(1)_{zz} values of the *c*-TRs in *bc*CDT and *cc*CDT were greater than those of the *b*-TRs (Table 1). The large value for the former can be attributed to an asymmetric fusing mode [65]. The MIC calculations performed using the GIMIC method corroborated the results of the NICS(1)_{zz} analyses. Though there were clockwise diatropic current flows over both the *b*- and *c*-TRs (Figure 2), the diatropic character of the *b*-TRs was stronger than that of the *c*-TRs. From the results of these analyses, we concluded that the local aromaticity of the *b*-TRs was preserved to some extent. The 4MRs of *syn-bb*CDT, *anti-bb*CDT, *bc*CDT, and *cc*CDT afforded respective positive NICS(1)_{zz} values of 52.5 ppm, 53.0 ppm, 29.2 ppm, and 17.8 ppm (Table 1). The former two values were close to that of the cyclobutadiene (Table S2). The GIMIC calculations confirmed counterclockwise paratropic current flows over the 4MRs (Figure 2). These analyses revealed that the anti-aromatic character of the 4MRs was comparable to that of the cyclobutadiene when the two *b*-TRs were fused [54,59,65].

Finally, we discuss the differences in the E_{Gap} values and total potential energies among the isomers. The E_{Gap} values of *syn-bb*CDT and *anti-bb*CDT were smaller than those of *bc*CDT and *cc*CDT (Table 2). When the number of fused *b*-TRs increased, the E_{Gap}

became smaller. The zero-point-corrected energies confirmed that *cc*CDT was the most stable. The relative total energy (E_{rel}) values of *syn-bb*CDT, *anti-bb*CDT, and *bc*CDT were 22.7 kcal/mol, 22.4 kcal/mol, and 7.0 kcal/mol, respectively, with respect to that of *cc*CDT. An increased number of fused *b*-TRs led to potential energy increments, probably because of the preserved anti-aromatic character of the 4MRs.

Table 2. E_{Gap} values for 1–4 and reference compounds *syn-bb*CDT, *anti-bb*CDT, *bc*CDT, *cc*CDT, and anti-kekulene, and E_{rel} values for *syn-bb*CDT, *anti-bb*CDT, *bc*CDT, and *cc*CDT.

Compound	E_{Gap} Value (eV)	E_{rel} ^a Value (kcal/mol)
<i>syn-bb</i> CDT	3.13	22.7
<i>anti-bb</i> CDT	3.23	22.4
<i>bc</i> CDT	3.94	7.0
<i>cc</i> CDT	4.35	0.0
anti-kekulene	2.77	—
1	2.74	—
2	2.85	—
3	2.67	—
4	2.78	—

^a Calculated from the zero-point-corrected total energies.

3.2. Structure and Aromaticity of Anti-Kekulene

As the next reference compound, we briefly discuss the geometry and aromaticity of anti-kekulene based on our calculations. The optimized geometry of anti-kekulene was very close to planar, with a D_6 symmetry group (Figure S2e). The benzene ring showed strong bond-length alternation (Figure 3a) with a difference of 0.101 Å, featuring a 1,3,5-cyclohexatriene-like part structure. The fused bond was elongated compared with that of benzene, whereas the non-shared bonds were shortened compared with those of benzene. The bridging bonds in the 4MR showed a single bond character. Moreover, the LOL- π isosurface of anti-kekulene confirmed that the π -electrons were localized at the three non-shared bonds (Figure 3b), in contrast to the full π -electron delocalization in benzene (Figure S3). The HOMA and MCI values of the fused benzene ring were smaller than those of benzene (Table 1 and Table S2). The cyclic π -electron conjugation of the fused benzene ring was significantly attenuated. The NICS(1)_{zz} values were 1.9 ppm, 24.3 ppm, and 16.6 ppm at the benzene ring, 4MR, and center of the macrocycle, respectively. The benzene rings showed a non-aromatic character. Notably, the paratropic character of the 4MR was attenuated compared with those of the cyclobutadiene and *bb*CDTs. The GIMIC calculation corroborated the results of the NICS(1)_{zz} analysis (Figure 3c). There was a paratropic current circuit in the 4MR, but no diatropic circuit in the benzene ring. Our GIMIC results were also in good agreement with the HLPM topological bond-current calculation reported by Dickens and Mallion [24].

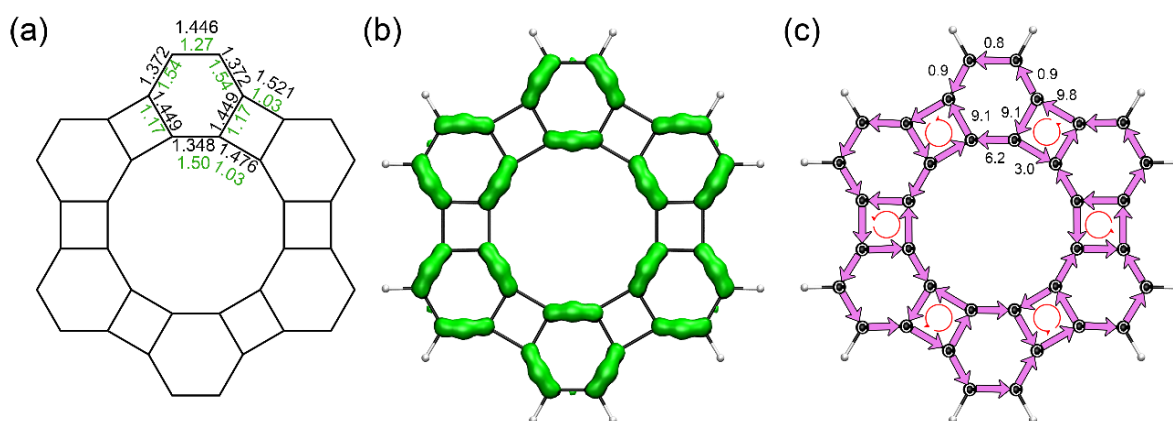


Figure 3. (a) Bond lengths (black numbers) and WBI values (green numbers), (b) LOL- π isosurface (isovalued: 0.55 a.u.), and (c) paths and strengths (nA/T) of MIC at each bond of anti-kekulene.

3.3. Structures, Electronic Properties, and Aromaticity of Thiophene Analogues of Anti-Kekulene

The geometry optimization of **1** with six thiophene rings afforded a bowl-shaped structure with a C_{6v} symmetry group, in contrast to its planar benzo-analogue, anti-kekulene (Figure 4a). This can be attributed to the shorter distance of the sulfur bridge. Upon enlargement of the cycles, the bowl depth became shallow. The MPP values of compounds **1**, **2**, and **3** were decreased upon ring enlargement (Figure 4b and Figure S2a–c). Compound **4** with nine thiophene rings adopted a nearly planar structure with a very small MPP value, similar to that of anti-kekulene. Next, we calculated the relative strain energies (E_{strain}) for **1–4** (Materials and Methods and Table S1). As shown in Figure 4b, the E_{strain} values became small when the molecules were close to planar, similar to previous reports on [n]circulenes [99] and thia[n]circulenes [42].

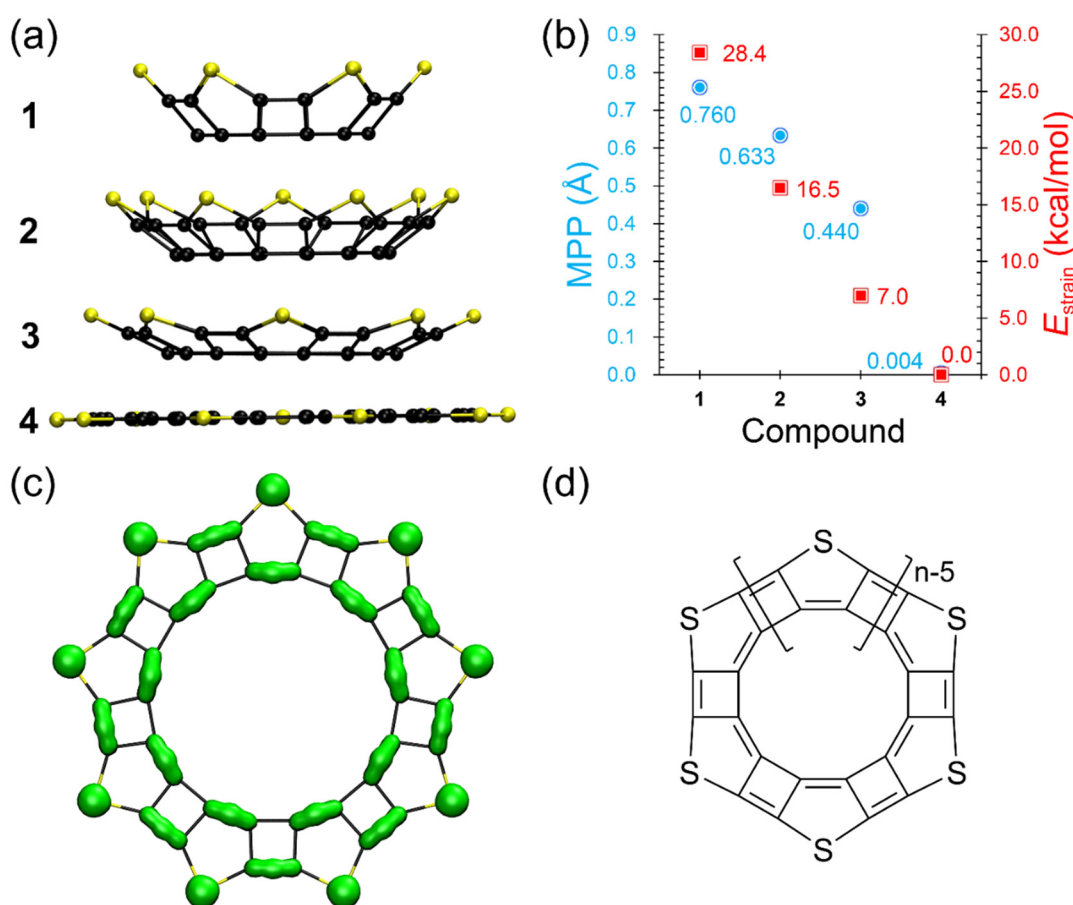


Figure 4. (a) Side view of the optimized structures of **1–4**. (b) MPP values (\AA ; blue; left y -axis) and relative strain energies (E_{strain} , kcal/mol; red; right y -axis) of **1–4**. (c) LOL- π isosurface (isovalue: 0.60 a.u.) of **4**. (d) Major electronic structures appearing in **1–4**.

The lengths of fused bond iii in **1–4** were slightly longer (by 0.1 \AA) than the shared bonds of the b -TR in the CDTs (Table 3). The WBI value of bond iii indicated its single bond character. On the other hand, the length and WBI values of bond iv confirmed its double bond character. The thiophene rings in **1–4** lost the original diene character of thiophene. It should be noted that bond vi in the 4MRs had a double bond character, as judged by its length and WBI values (1.38 \AA and 1.52–1.53, respectively). The LOL- π analyses for **1–4** supported the above conclusions, as the isosurfaces localized at bonds iv and vi (Figures 4c and S4). These bonding characters were distinctly different from those of the bb CDTs. On the basis of these results, we suggest the significant contribution of a quinoidal electronic structure in **1–4** (Figure 4d) [68,69]. Notably, a theoretical study

by Fabian and Hartmann reported no contribution of such a quinoid structure in neutral cyclo[n]thiophenes ($n \geq 5$) [100].

Table 3. Bond lengths (Å), WBI values, and calculated current strengths (nA/T) for 1–4.

Compound		Bond Position ^a						
		i	ii	iii	iv	v	vi	vii
1	bond length (Å)	1.781	1.781	1.494	1.334	1.494	1.379	1.481
	WBI value	1.08	1.08	1.02	1.64	1.02	1.53	1.02
	current strength (nA/T)	0.91	0.91	2.89	0.96	2.89	1.68	1.29
2	bond length (Å)	1.778	1.778	1.493	1.333	1.493	1.378	1.479
	WBI value	1.09	1.09	1.02	1.64	1.02	1.53	1.02
	current strength (nA/T)	1.40	1.40	3.44	0.99	3.44	2.46	2.47
3	bond length (Å)	1.777	1.777	1.492	1.332	1.493	1.378	1.479
	WBI value	1.09	1.09	1.02	1.64	1.02	1.52	1.02
	current strength (nA/T)	1.72	1.72	4.32	1.52	4.32	3.01	2.61
4	bond length (Å)	1.773	1.773	1.493	1.334	1.493	1.375	1.483
	WBI value	1.09	1.09	1.02	1.65	1.02	1.52	1.01
	current strength (nA/T)	2.13	2.13	5.10	1.56	5.10	3.43	3.29

^a Bond positions are included in Figure 1.

The HOMA values of the fused thiophene rings of 1–4 were very small (Table 1). The MCI values also became smaller than those of the fused thiophene rings of the *bb*CDTs. Obviously, the cyclic π -conjugation in the fused thiophene rings in 1–4 was significantly attenuated. The NICS(1)_{zz} values of the thiophene rings in 1–4 were close to zero, indicating a negligible diatropic character. Moreover, the NICS(1)_{zz} values of the 4MRs in 1–4 indicated significant attenuation of paratropic character compared with the *bb*CDTs and anti-kekulene. The NICS(1)_{zz} values calculated at the macrocyclic centrum were small and positive. According to the current paths obtained from the GIMIC calculations (Figure 5), there were weak diatropic and paratropic current circuits in the thiophene rings and 4MRs. The weak current strengths agreed with the small NICS values (Table 3). Overall, both the aromaticity and anti-aromaticity of the thiophene rings and 4MRs in 1–4 were considerably attenuated compared with those of the *bb*CDTs. We attribute this to the major contribution of a quinoidal electronic structure in 1–4. In both anti-kekulene and its thiopheno-analogues, to reduce the electron density at the shared bonds, π -electrons are localized at the non-shared bonds. For the fused benzene rings of anti-kekulene, π -electrons can be localized at three of the four non-shared bonds by adopting a 1,3,5-hexatriene-like part structure. On the other hand, it is impossible to adopt such an electronic structure in the five-membered thiophene rings of 1–4. Instead, the quinoidal electronic structure appeared in compounds 1–4.

Upon increasing the number of the fused thiophene ring, the MPP and E_{strain} values were reduced and the local aromaticity and anti-aromaticity of the thiophene ring and 4MR gradually recovered (Tables 1 and 3). We concluded that this was because of the planarization of the molecular frameworks. It should be noted that there was only a small change in the E_{Gap} values among 1–4 (Table 2), indicating very limited π -electron delocalization through the macrocyclic pathway.

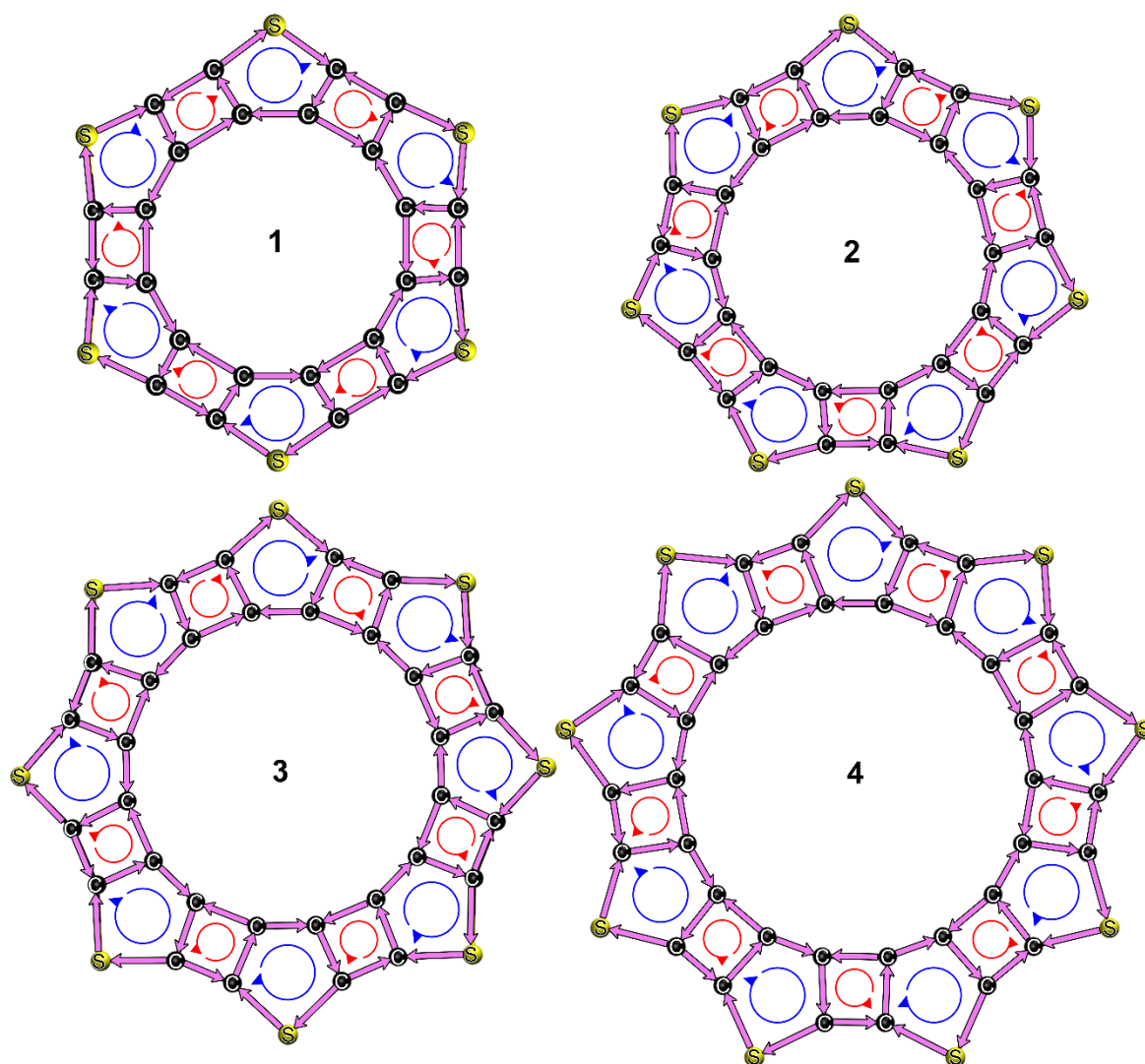


Figure 5. The MIC paths in 1–4. The current strengths of each bond are summarized in Table 3.

4. Conclusions

We predicted the structures, electronic properties, and aromaticity of novel thiophene analogues of cyclic [n]phenylenes 1–4 together with four CDTs and anti-kekulene, as reference compounds.

Among the four CDTs, the *b*-TRs and 4MR in the *bb*CDTs preserved local aromaticity and anti-aromaticity, whereas the *c*-TRs and 4MR in *cc*CDT showed attenuated local aromaticity and anti-aromaticity. The fusion of the *b*-TRs to the 4MR led to a reduction in E_{Gap} , as well as an increment in total potential energy. For the other reference compound, anti-kekulene, the results of our calculations support the findings of previous studies, i.e., local paratropic features at the 4MRs.

The geometry optimizations of 1–3 afforded bowl-shaped structures, whereas that of 4 gave a nearly planar structure. The molecular planarity increased upon ring enlargement. The fused bonds of 1–4 were elongated, in contrast to those of the *bb*CDTs. Moreover, the structural features of compounds 1–4 indicated the significant contribution of a quinoidal electronic structure. We attribute this to strong π -electron localization at the non-fused bonds of the thiophene rings and 4MRs. Several aromaticity indices proved that the local cyclic conjugations in the thiophene rings were significantly attenuated and featured a non-aromatic character. Moreover, the anti-aromaticity of the 4MRs decreased compared with that of the reference compounds. This we again attribute to the significant contribution of the quinoidal electronic structure.

The results presented here provide a fundamental understanding of the aromatic and electronic nature of a cyclic π -conjugated system containing cyclobutadienothiophene, and will be useful for the further design of novel functional polycyclic organic molecules.

Supplementary Materials: The following supporting information can be downloaded at: <https://www.mdpi.com/article/10.3390/chemistry4040102/s1>, Supplementary File S1: Supporting information for this paper including the details of strain energy calculations, MPP analysis, structures and aromaticity of benzene, thiophene, and cyclobutadiene, NICS(1)_{zz} values of the concave face, LOL- π isosurfaces of 1–3, molecular orbital diagrams, the signed modules of current densities, calculated atomic charge, and cartesian coordinates. References [101–104] described in the main text are cited in the Supplementary File S1.

Author Contributions: Conceptualization, S.H.; methodology, S.H.; software, S.H.; validation, S.H. and K.T.; formal analysis, S.H.; investigation, S.H. and K.T.; resources, K.T.; data curation, S.H.; writing—original draft preparation, S.H.; writing—review and editing, S.H. and K.T.; visualization, S.H. and K.T.; supervision, K.T.; project administration, K.T.; funding acquisition, K.T. All authors have read and agreed to the published version of the manuscript.

Funding: This research was funded by the Tokuyama Science Foundation.

Data Availability Statement: Not applicable.

Acknowledgments: K.T. acknowledges the Tokuyama Science Foundation.

Conflicts of Interest: The authors declare no conflict of interest.

References

1. Hong, C.; Baltazar, J.; Tovar, J.D. Manifestations of Antiaromaticity in Organic Materials: Case Studies of Cyclobutadiene, Borole, and Pentalene. *Eur. J. Org. Chem.* **2022**, *2022*, e202101343. [CrossRef]
2. Miyoshi, H.; Sugiura, R.; Kishi, R.; Spisak, S.N.; Wei, Z.; Muranaka, A.; Uchiyama, M.; Kobayashi, N.; Chatterjee, S.; Ie, Y.; et al. Dianion and Dication of Tetracyclopentatetraphenylene as Decoupled Annulene-within-an-Annulene Models. *Angew. Chem. Int. Ed.* **2022**, *61*, e202115316. [CrossRef]
3. Konishi, A.; Okada, Y.; Kishi, R.; Nakano, M.; Yasuda, M. Enhancement of Antiaromatic Character via Additional Benzoannulation into Dibenzo[*a,f*]Pentalene: Syntheses and Properties of Benzo[*a*]Naphtho[2,1-*f*]Pentalene and Dinaphtho[2,1-*a,f*]Pentalene. *J. Am. Chem. Soc.* **2019**, *141*, 560–571. [CrossRef]
4. Esser, B.; Wössner, J.S.; Hermann, M. Conjugated Nanohoops with Dibenzo[*a,e*]Pentalenes as Nonalternant and Antiaromatic π -Systems. *Synlett* **2022**, *33*, 737–753. [CrossRef]
5. Kalapos, P.P.; Mayer, P.J.; Gazdag, T.; Demeter, A.; Oruganti, B.; Durbej, B.; London, G. Photoswitching of Local (Anti)Aromaticity in Biphenylene-Based Diarylethene Molecular Switches. *J. Org. Chem.* **2022**, *87*, 9532–9542. [CrossRef]
6. Liu, J.; Ma, J.; Zhang, K.; Ravat, P.; Machata, P.; Avdoshenko, S.; Hennersdorf, F.; Komber, H.; Pisula, W.; Weigand, J.J.; et al. π -Extended and Curved Antiaromatic Polycyclic Hydrocarbons. *J. Am. Chem. Soc.* **2017**, *139*, 7513–7521. [CrossRef]
7. Akahori, S.; Kaga, A.; Kim, J.; Yorimitsu, H.; Kim, D.; Shinokubo, H.; Miyake, Y. Protonation-Induced Antiaromaticity in Octaaza[8]Circulenes: Cyclooctatetraene Scaffolds Constrained with Four Amidine Moieties. *Chem. Asian J.* **2022**, *17*, e202200244. [CrossRef]
8. Tahara, K.; Kozuma, H.; Venkatesh, V.; Ryomura, E.; Miyoshi, H.; Nakamachi, K.; Kishi, R.; Takahashi, H.; Nakano, M.; Tobe, Y. Generation of Aromatic (Dehydro)Benzoannulene Dications Stabilized by Platinum Catecholate Complexes. *ChemPlusChem* **2017**, *82*, 1052–1056. [CrossRef]
9. Takano, H.; Ito, T.; Kanyiva, K.S.; Shibata, T. Recent Advances of Biphenylene: Synthesis, Reactions and Uses. *Eur. J. Org. Chem.* **2019**, *2019*, 2871–2883. [CrossRef]
10. Lothrop, W.C. Biphenylene. *J. Am. Chem. Soc.* **1941**, *63*, 1187–1191. [CrossRef]
11. Miljanić, O.Š.; Vollhardt, K.P.C. [N]Phenylenes: A Novel Class of Cyclohexatrienoid Hydrocarbon. In *Carbon-Rich Compounds: From Molecules to Materials*; Haley, M.M., Tykwinski, R.R., Eds.; Wiley-VCH Verlag GmbH & Co. KGaA: Weinheim, Germany, 2006; pp. 140–197. [CrossRef]
12. Berris, B.C.; Hovakeemian, G.H.; Lai, Y.H.; Mestdagh, H.; Vollhardt, K.P.C. A New Approach to the Construction of Biphenylenes by the Cobalt-Catalyzed Cocyclization of *o*-Diethynylbenzenes with Alkynes. Application to an Iterative Approach to [3]Phenylene, the First Member of a Novel Class of Benzocyclobutadienoid Hydrocarbons. *J. Am. Chem. Soc.* **1985**, *107*, 5670–5687. [CrossRef]
13. Diercks, R.; Vollhardt, K.P.C. Novel Synthesis of the Angular [3]Phenylene (Terphenylene) by Cobalt-Catalyzed Cyclization of Bis(2-Ethynylphenyl)Ethyne: A Molecule with an Internal Cyclohexatriene Ring. *Angew. Chem. Int. Ed. Engl.* **1986**, *25*, 266–268. [CrossRef]

14. Diercks, R.; Vollhardt, K.P.C. Tris(Benzocyclobutadieno)Benzene, the Triangular [4]Phenylene with a Completely Bond-Fixed Cyclohexatriene Ring: Cobalt-Catalyzed Synthesis from Hexaethynylbenzene and Thermal Ring Opening to 1,2:5,6:9,10-Tribenzo-3,4,7,8,11,12-Hexadehydro[12]Annulene. *J. Am. Chem. Soc.* **1986**, *108*, 3150–3152. [[CrossRef](#)]
15. Gershoni-Poranne, R.; Gibson, C.M.; Fowler, P.W.; Stanger, A. Concurrence between Current Density, Nucleus-Independent Chemical Shifts, and Aromatic Stabilization Energy: The Case of Isomeric [4]- and [5]Phenylenes. *J. Org. Chem.* **2013**, *78*, 7544–7553. [[CrossRef](#)]
16. Radenković, S.; Tošović, J.; Havenith, R.W.A.; Bultinck, P. Ring Currents in Benzo- and Benzocyclobutadieno-Annulated Biphenylene Derivatives. *ChemPhysChem* **2015**, *16*, 216–222. [[CrossRef](#)] [[PubMed](#)]
17. Holmes, D.; Kumaraswamy, S.; Matzger, A.J.; Vollhardt, K.P.C. On the Nature of Nonplanarity in the [N]Phenylenes. *Chem. Eur. J.* **1999**, *5*, 3399–3412. [[CrossRef](#)]
18. Dosche, C.; Mickler, W.; Löhmansröben, H.-G.; Agenet, N.; Vollhardt, K.P.C. Photoinduced Electron Transfer in [N]Phenylenes. *J. Photochem. Photobiol. A* **2007**, *188*, 371–377. [[CrossRef](#)]
19. Schulman, J.M.; Disch, R.L. Theoretical Studies of the [N]Phenylenes. *J. Am. Chem. Soc.* **1996**, *118*, 8470–8474. [[CrossRef](#)]
20. Schulman, J.M.; Disch, R.L.; Jiao, H.; Schleyer, P.v.R. Chemical Shifts of the [N]Phenylenes and Related Compounds. *J. Phys. Chem. A* **1998**, *102*, 8051–8055. [[CrossRef](#)]
21. Anjalikrishna, P.K.; Gadre, S.R.; Suresh, C.H. Antiaromaticity–Aromaticity Interplay in Fused Benzenoid Systems Using Molecular Electrostatic Potential Topology. *J. Phys. Chem. A* **2021**, *125*, 5999–6012. [[CrossRef](#)]
22. Babić, D.; Trinajstić, N. Kekulene and Antikekulene. *J. Mol. Struct. THEOCHEM* **1994**, *314*, 321–327. [[CrossRef](#)]
23. Aihara, J. A Simple Method for Estimating the Superaromatic Stabilization Energy of a Super-Ring Molecule. *J. Phys. Chem. A* **2008**, *112*, 4382–4385. [[CrossRef](#)] [[PubMed](#)]
24. Dickens, T.K.; Mallion, R.B. Topological Ring-Current Assessment of the ‘Annulene-within-an-Annulene’ Model in [N]-Circulenes and Some Structures Related to Kekulene. *Chem. Phys. Lett.* **2011**, *517*, 98–102. [[CrossRef](#)]
25. Gribanova, T.N.; Minyaev, R.M.; Minkin, V.I. Parquet Compounds on the Basis of Eight- and Twelve-Membered Structure Blocks: Quantum-Chemical Study. *Russ. J. Org. Chem.* **2016**, *52*, 268–282. [[CrossRef](#)]
26. Randić, M.; Balaban, A.T.; Plavšić, D. Applying the Conjugated Circuits Method to Clar Structures of [n]Phenylenes for Determining Resonance Energies. *Phys. Chem. Chem. Phys.* **2011**, *13*, 20644–20648. [[CrossRef](#)]
27. Miyoshi, H.; Nobusue, S.; Shimizu, A.; Tobe, Y. Non-Alternant Non-Benzenoid Kekulenes: The Birth of a New Kekulene Family. *Chem. Soc. Rev.* **2015**, *44*, 6560–6577. [[CrossRef](#)]
28. Dickens, T.K.; Mallion, R.B. An Analysis of Topological Ring-Currents and Their Use in Assessing the Annulene-within-an-Annulene Model for Super-Ring Conjugated Systems. *Croat. Chem. Acta* **2013**, *86*, 387–406. [[CrossRef](#)]
29. Dickens, T.K.; Mallion, R.B. Topological Ring-Currents in Conjugated Systems. *MATCH Commun. Math. Comput. Chem.* **2016**, *76*, 297–356.
30. Yates, K. Hückel Molecular Orbital Theory. In *Hückel Molecular Orbital Theory*; Academic Press Inc.: New York, NY, USA, 1978; pp. 27–87. [[CrossRef](#)]
31. London, F. Théorie Quantique Des Courants Interatomiques Dans Les Combinaisons Aromatiques. *J. Phys. Radium* **1937**, *8*, 397–409. [[CrossRef](#)]
32. Eickmeier, C.; Junga, H.; Matzger, A.J.; Scherhag, F.; Shim, M.; Vollhardt, K.P.C. 5,6,11,12,17,18-Hexadehydro-1,4,7,10,13,16-Hexaethynyltribenzo[*a,e,i*]Cyclododecene: Synthesis and CpCo-Catalyzed Cycloisomerization to the First Superdelocalized Oligophenylenes. *Angew. Chem. Int. Ed. Engl.* **1997**, *36*, 2103–2108. [[CrossRef](#)]
33. Fonari, A.; Röder, J.C.; Shen, H.; Timofeeva, T.V.; Vollhardt, K.P.C. Toward Antikekulene: Angular 1,2-Di-, 2,3-Di-, and 1,2,15,16-Tetrachloro[6]Phenylene. *Synlett* **2014**, *25*, 2429–2433. [[CrossRef](#)]
34. Dahlmann, U.; Vollhardt, K.P.C. Oligoether-Substituted Derivatives of Carbon-Rich 1,4,7,10,13,16-Hexaethynyltribenzo[*a,e,i*]Cyclododeca-5,11,17-Triyne (C₃₆H₁₂) and 1,4,9,12-Tetrakis(Ethynyl)Dibenzo[*a,g*]Cyclododeca-5,7,13,15-Tetrayne (C₂₈H₈): Potential Precursors to the Circular [6]Phenylene (‘Antikekulene’) Frame. *Synthesis* **2020**, *52*, 1287–1300. [[CrossRef](#)]
35. Mamada, M.; Yamashita, Y. S-Containing Polycyclic Heteroarenes: Thiophene-Fused and Thiadiazole-Fused Arenes as Organic Semiconductors. In *Polycyclic Arenes and Heteroarenes: Synthesis, Properties, and Applications*; Miao, Q., Ed.; Wiley-VCH Verlag GmbH & Co. KGaA: Weinheim, Germany, 2015; pp. 277–308. [[CrossRef](#)]
36. Okamoto, T.; Mitsui, C.; Yamagishi, M.; Nakahara, K.; Soeda, J.; Hirose, Y.; Miwa, K.; Sato, H.; Yamano, A.; Matsushita, T.; et al. V-Shaped Organic Semiconductors with Solution Processability, High Mobility, and High Thermal Durability. *Adv. Mater.* **2013**, *25*, 6392–6397. [[CrossRef](#)]
37. Irie, M.; Fukaminato, T.; Matsuda, K.; Kobatake, S. Photochromism of Diarylethene Molecules and Crystals: Memories, Switches, and Actuators. *Chem. Rev.* **2014**, *114*, 12174–12277. [[CrossRef](#)] [[PubMed](#)]
38. Shinohara, K.; Sannohe, Y.; Kaieda, S.; Tanaka, K.; Osuga, H.; Tahara, H.; Xu, Y.; Kawase, T.; Bando, T.; Sugiyama, H. A Chiral Wedge Molecule Inhibits Telomerase Activity. *J. Am. Chem. Soc.* **2010**, *132*, 3778–3782. [[CrossRef](#)] [[PubMed](#)]
39. di Maria, F.; Zangoli, M.; Barbarella, G. Supramolecular Thiophene-Based Materials: A Few Examples of the Interplay between Synthesis, Optoelectronic Properties and Applications. *Org. Mater.* **2021**, *3*, 321–336. [[CrossRef](#)]
40. Ueda, M.; Aoki, T.; Akiyama, T.; Nakamuro, T.; Yamashita, K.; Yanagisawa, H.; Nureki, O.; Kikkawa, M.; Nakamura, E.; Aida, T.; et al. Alternating Heterochiral Supramolecular Copolymerization. *J. Am. Chem. Soc.* **2021**, *143*, 5121–5126. [[CrossRef](#)]

41. Li, G.; Gopalakrishna, T.Y.; Phan, H.; Heng, T.S.; Ding, J.; Wu, J. From Open-Shell Singlet Diradicaloid to Closed-Shell Global Antiaromatic Macrocycles. *Angew. Chem. Int. Ed.* **2018**, *57*, 7166–7170. [[CrossRef](#)]
42. Chernichenko, K.Y.; Sumerin, V.V.; Shpanchenko, R.V.; Balenkova, E.S.; Nenajdenko, V.G. “Sulflower”: A New Form of Carbon Sulfide. *Angew. Chem. Int. Ed.* **2006**, *45*, 7367–7370. [[CrossRef](#)]
43. Sakamoto, Y.; Suzuki, T. Tetrabenzo[8]Circulene: Aromatic Saddles from Negatively Curved Graphene. *J. Am. Chem. Soc.* **2013**, *135*, 14074–14077. [[CrossRef](#)]
44. Feng, C.-N.; Kuo, M.-Y.; Wu, Y.-T. Synthesis, Structural Analysis, and Properties of [8]Circulenes. *Angew. Chem. Int. Ed.* **2013**, *52*, 7791–7794. [[CrossRef](#)] [[PubMed](#)]
45. Fujimoto, T.; Suizu, R.; Yoshikawa, H.; Awaga, K. Molecular, Crystal, and Thin-Film Structures of Octathio[8]Circulene: Release of Antiaromatic Molecular Distortion and Lamellar Structure of Self-Assembling Thin Films. *Chem. Eur. J.* **2008**, *14*, 6053–6056. [[CrossRef](#)] [[PubMed](#)]
46. Fujimoto, T.; Matsushita, M.M.; Awaga, K. Ionic-Liquid Component Dependence of Carrier Injection and Mobility for Electric-Double-Layer Organic Thin-Film Transistors. *J. Phys. Chem. C* **2012**, *116*, 5240–5245. [[CrossRef](#)]
47. Fujimoto, T.; Matsushita, M.M.; Awaga, K. Dual-Gate Field-Effect Transistors of Octathio[8]Circulene Thin-Films with Ionic Liquid and SiO₂ Gate Dielectrics. *Appl. Phys. Lett.* **2010**, *97*, 123303. [[CrossRef](#)]
48. Takimiya, K.; Shinamura, S.; Osaka, I.; Miyazaki, E. Thienoacene-Based Organic Semiconductors. *Adv. Mater.* **2011**, *23*, 4347–4370. [[CrossRef](#)]
49. Dressler, J.J.; Teraoka, M.; Espejo, G.L.; Kishi, R.; Takamuku, S.; Gómez-García, C.J.; Zakharov, L.N.; Nakano, M.; Casado, J.; Haley, M.M. Thiophene and Its Sulfur Inhibit Indenoindenodibenzothiophene Diradicals from Low-Energy Lying Thermal Triplets. *Nat. Chem.* **2018**, *10*, 1134–1140. [[CrossRef](#)] [[PubMed](#)]
50. Usuba, J.; Fukazawa, A. Thiophene-Fused 1,4-Diazapentalene: A Stable C=N-Containing Π -Conjugated System with Restored Antiaromaticity. *Chem. Eur. J.* **2021**, *27*, 16127–16134. [[CrossRef](#)]
51. Aita, K.; Ohmae, T.; Takase, M.; Nomura, K.; Kimura, H.; Nishinaga, T. Dithieno[3,4-*b*:3',4'-*d*]Thiophene-Annelated Antiaromatic Planar Cyclooctatetraene with Olefinic Protons. *Org. Lett.* **2013**, *15*, 3522–3525. [[CrossRef](#)]
52. Ohmae, T.; Nishinaga, T.; Wu, M.; Iyoda, M. Cyclic Tetrathiophenes Planarized by Silicon and Sulfur Bridges Bearing Antiaromatic Cyclooctatetraene Core: Syntheses, Structures, and Properties. *J. Am. Chem. Soc.* **2010**, *132*, 1066–1074. [[CrossRef](#)]
53. Fringuelli, F.; Marino, G.; Taticchi, A.; Grandolini, G. A Comparative Study of the Aromatic Character of Furan, Thiophen, Selenophen, and Tellurophen. *J. Chem. Soc. Perkin Trans.* **1974**, *2*, 332–337. [[CrossRef](#)]
54. Frederickson, C.K.; Zakharov, L.N.; Haley, M.M. Modulating Paratropicity Strength in Diareno-Fused Antiaromatics. *J. Am. Chem. Soc.* **2016**, *138*, 16827–16838. [[CrossRef](#)] [[PubMed](#)]
55. Jones, R.R.; Brown, J.M.; Sondheimer, F. Annelated 14 π -Electron Systems. The Synthesis of a Dimethylbisdehydro[14]Annuleno[*c*]Thiophene, -[*b*]Thiophene and -[*b*]Furan. *Tetrahedron Lett.* **1975**, *16*, 4183–4186. [[CrossRef](#)]
56. Boydston, A.J.; Haley, M.M.; Williams, R.V.; Armantrout, J.R. Diatropicity of 3,4,7,8,9,10,13,14-Octadehydro[14]Annulenes: A Combined Experimental and Theoretical Investigation. *J. Org. Chem.* **2002**, *67*, 8812–8819. [[CrossRef](#)] [[PubMed](#)]
57. O'Connor, M.J.; Yelle, R.B.; Zakharov, L.N.; Haley, M.M. Structure–Property Investigations of Conjugated Thiophenes Fused onto a Dehydro[14]Annulene Scaffold. *J. Org. Chem.* **2008**, *73*, 4424–4432. [[CrossRef](#)]
58. Sarkar, A.; Haley, M.M. Synthesis and Characterization of Dehydrothieno[18]Annulenes. *Chem. Commun.* **2000**, 1733–1734. [[CrossRef](#)]
59. Ohtomo, Y.; Ishiwata, K.; Hashimoto, S.; Kuroiwa, T.; Tahara, K. Revisiting Dehydrothiopheno[12]Annulenes: Synthesis, Electronic Properties, and Aromaticity. *J. Org. Chem.* **2021**, *86*, 13198–13211. [[CrossRef](#)]
60. Usuba, J.; Hayakawa, M.; Yamaguchi, S.; Fukazawa, A. Dithieno[*a,e*]Pentalenes: Highly Antiaromatic Yet Stable π -Electron Systems without Bulky Substituents. *Chem. Eur. J.* **2021**, *27*, 1638–1647. [[CrossRef](#)]
61. Gazdag, T.; Mayer, P.J.; Kalapos, P.P.; Holczbauer, T.; El Bakouri, O.; London, G. Unsymmetrical Thienopentalenes: Synthesis, Optoelectronic Properties, and (Anti)Aromaticity Analysis. *ACS Omega* **2022**, *7*, 8336–8349. [[CrossRef](#)]
62. Engelhardt, V.; Gabriel Garcia, J.; Hubaud, A.A.; Lyssenko, K.A.; Spyroudis, S.; Timofeeva, T.V.; Tongwa, P.; Vollhardt, K.P.C. The Cobalt-Way to Heterophenylenes: Syntheses of 2-Thianorbiphenylenes, Monoazabiphenylenes, and Linear 1-Aza[3]Phenylene {biphenyleno[2,3-*a*]Cyclobuta[1,2-*b*]Pyridine}. *Synlett* **2011**, *2011*, 280–284. [[CrossRef](#)]
63. Garratt, P.J.; Vollhardt, K.P.C. Benzo[3,4]Cyclobuta[1,2-*c*]Thiophen (2-Thianorbiphenylene). *J. Chem. Soc. D* **1970**, 109. [[CrossRef](#)]
64. Barton, J.W.; Lapham, D.J. Benzo[3,4]Cyclobuta[1,2-*b*]Thiophene. *Tetrahedron Lett.* **1979**, *20*, 3571–3572. [[CrossRef](#)]
65. Hashimoto, S.; Tahara, K. Theoretical Study on the Geometry, Aromaticity, and Electronic Properties of Benzo[3,4]Cyclobutathiophenes and Their Homologues. *J. Org. Chem.* **2019**, *84*, 9850–9858. [[CrossRef](#)] [[PubMed](#)]
66. Párkányi, C.; Huang, D.-L.; Kalsotra, B.L.; Jeffries, A.T.I.; Lloyd, W.D. Attempted Synthesis of the Dithiophene Analogs of Biphenylene. *Bull. Soc. Chim. Belg.* **1987**, *96*, 237–244. [[CrossRef](#)]
67. Shepherd, M.K. Cyclobuta[1,2-*c*:3,4-*c'*]Dithiophene. *J. Chem. Soc. Chem. Commun.* **1985**, 880–881. [[CrossRef](#)]
68. Ponce Ortiz, R.; Casado, J.; Rodríguez González, S.; Hernández, V.; López Navarrete, J.T.; Viruela, P.M.; Ortí, E.; Takimiya, K.; Otsubo, T. Quinoidal Oligothiophenes: Towards Biradical Ground-State Species. *Chem. Eur. J.* **2010**, *16*, 470–484. [[CrossRef](#)]
69. Takahashi, T.; Matsuoka, K.; Takimiya, K.; Otsubo, T.; Aso, Y. Extensive Quinoidal Oligothiophenes with Dicyanomethylene Groups at Terminal Positions as Highly Amphoteric Redox Molecules. *J. Am. Chem. Soc.* **2005**, *127*, 8928–8929. [[CrossRef](#)]

70. Frisch, M.J.; Trucks, G.W.; Schlegel, H.B.; Scuseria, G.E.; Robb, M.A.; Cheeseman, J.R.; Scalmani, G.; Barone, V.; Petersson, G.A.; Nakatsuji, H.; et al. *Gaussian16*; Revision A.01; Gaussian, Inc.: Wallingford, CT, USA, 2016.
71. Grimme, S.; Antony, J.; Ehrlich, S.; Krieg, H. A Consistent and Accurate Ab Initio Parametrization of Density Functional Dispersion Correction (DFT-D) for the 94 Elements H-Pu. *J. Chem. Phys.* **2010**, *132*, 154104. [[CrossRef](#)]
72. Grimme, S.; Ehrlich, S.; Goerigk, L. Effect of the Damping Function in Dispersion Corrected Density Functional Theory. *J. Comput. Chem.* **2011**, *32*, 1456–1465. [[CrossRef](#)]
73. Boese, R.; Bläser, D.; Latz, R. Redetermination of Biphenylene at 130K. *Acta Crystallogr. Sect. C Cryst. Struct. Commun.* **1999**, *55*, IUC9900067. [[CrossRef](#)]
74. Bauernschmitt, R.; Ahlrichs, R. Stability Analysis for Solutions of the Closed Shell Kohn–Sham Equation. *J. Chem. Phys.* **1996**, *104*, 9047–9052. [[CrossRef](#)]
75. Dennington, R.; Keith, T.A.; Millam, J.M. *GaussView (Ver. 6. 0. 16)*; Semichem Inc.: Shawnee Mission, KS, USA, 2016.
76. Humphrey, W.; Dalke, A.; Schulten, K. VMD: Visual Molecular Dynamics. *J. Mol. Graphics* **1996**, *14*, 33–38. [[CrossRef](#)]
77. Lu, T. Simple, Reliable, and Universal Metrics of Molecular Planarity. *J. Mol. Model.* **2021**, *27*, 263. [[CrossRef](#)] [[PubMed](#)]
78. Lu, T.; Chen, F. Multiwfn: A Multifunctional Wavefunction Analyzer. *J. Comput. Chem.* **2012**, *33*, 580–592. [[CrossRef](#)] [[PubMed](#)]
79. Kruszewski, J.; Krygowski, T.M. Definition of Aromaticity Basing on the Harmonic Oscillator Model. *Tetrahedron Lett.* **1972**, *13*, 3839–3842. [[CrossRef](#)]
80. Krygowski, T.M. Crystallographic Studies of Inter- and Intramolecular Interactions Reflected in Aromatic Character of π -Electron Systems. *J. Chem. Inf. Comput. Sci.* **1993**, *33*, 70–78. [[CrossRef](#)]
81. Bultinck, P.; Ponec, R.; Van Damme, S. Multicenter Bond Indices as a New Measure of Aromaticity in Polycyclic Aromatic Hydrocarbons. *J. Phys. Org. Chem.* **2005**, *18*, 706–718. [[CrossRef](#)]
82. Casademont-Reig, I.; Ramos-Cordoba, E.; Torrent-Sucarrat, M.; Matito, E. Aromaticity Descriptors Based on Electron Delocalization. In *Aromaticity: Modern Computational Methods and Applications*; Fernández, I., Ed.; Elsevier: Amsterdam, The Netherlands, 2021; pp. 235–259. [[CrossRef](#)]
83. Reed, A.E.; Weinstock, R.B.; Weinhold, F. Natural Population Analysis. *J. Chem. Phys.* **1985**, *83*, 735–746. [[CrossRef](#)]
84. Glendening, E.D.; Reed, A.E.; Carpenter, J.E.; Weinhold, F. *NBO Version 3.1*; Theoretical Chemistry Institute, University of Wisconsin: Madison, WI, USA, 1998.
85. Wiberg, K.B. Application of the Pople-Santry-Segal CNDO Method to the Cyclopropylcarbinyl and Cyclobutyl Cation and to Bicyclobutane. *Tetrahedron* **1968**, *24*, 1083–1096. [[CrossRef](#)]
86. Schmider, H.L.; Becke, A.D. Chemical Content of the Kinetic Energy Density. *J. Mol. Struct. THEOCHEM* **2000**, *527*, 51–61. [[CrossRef](#)]
87. Steinmann, S.N.; Mo, Y.; Corminboeuf, C. How Do Electron Localization Functions Describe π -Electron Delocalization? *Phys. Chem. Chem. Phys.* **2011**, *13*, 20584–20592. [[CrossRef](#)]
88. Schleyer, P.v.R.; Maerker, C.; Dransfeld, A.; Jiao, H.; van Eikema Hommes, N.J.R. Nucleus-Independent Chemical Shifts: A Simple and Efficient Aromaticity Probe. *J. Am. Chem. Soc.* **1996**, *118*, 6317–6318. [[CrossRef](#)] [[PubMed](#)]
89. Fallah-Bagher-Shadaei, H.; Wannere, C.S.; Corminboeuf, C.; Puchta, R.; Schleyer, P.v.R. Which NICS Aromaticity Index for Planar π Rings Is Best? *Org. Lett.* **2006**, *8*, 863–866. [[CrossRef](#)] [[PubMed](#)]
90. Jusélius, J.; Sundholm, D.; Gauss, J. Calculation of Current Densities Using Gauge-Including Atomic Orbitals. *J. Chem. Phys.* **2004**, *121*, 3952–3963. [[CrossRef](#)]
91. Fliegl, H.; Taubert, S.; Lehtonen, O.; Sundholm, D. The Gauge Including Magnetically Induced Current Method. *Phys. Chem. Chem. Phys.* **2011**, *13*, 20500–20518. [[CrossRef](#)]
92. Myrvold, W.; Fowler, P.W.; Clarke, J. Partitioning Hückel–London Currents into Cycle Contributions. *Chemistry* **2021**, *3*, 1138–1156. [[CrossRef](#)]
93. Aihara, J. Graph Theory of Ring-Current Diamagnetism. *Bull. Chem. Soc. Jpn.* **2018**, *91*, 274–303. [[CrossRef](#)]
94. Pasquarello, A.; Schlüter, M.; Haddon, R.C. Ring Currents in Topologically Complex Molecules: Application to C₆₀, C₇₀, and Their Hexa-Anions. *Phys. Rev. A* **1993**, *47*, 1783–1789. [[CrossRef](#)]
95. Lazzeretti, P.; Malagoli, M.; Zanasi, R. Computational Approach to Molecular Magnetic Properties by Continuous Transformation of the Origin of the Current Density. *Chem. Phys. Lett.* **1994**, *220*, 299–304. [[CrossRef](#)]
96. Monaco, G.; Summa, F.F.; Zanasi, R. Program Package for the Calculation of Origin-Independent Electron Current Density and Derived Magnetic Properties in Molecular Systems. *J. Chem. Inf. Model.* **2021**, *61*, 270–283. [[CrossRef](#)]
97. Rauhalahhti, M.; Taubert, S.; Sundholm, D.; Liégeois, V. Calculations of Current Densities for Neutral and Doubly Charged Persubstituted Benzenes Using Effective Core Potentials. *Phys. Chem. Chem. Phys.* **2017**, *19*, 7124–7131. [[CrossRef](#)]
98. Ayachit, U. *The ParaView Guide: A Parallel Visualization Application*; Kitware, Inc.: New York, NY, USA, 2015; ISBN 978-1-930934-30-6.
99. Christoph, H.; Grunenberg, J.; Hopf, H.; Dix, I.; Jones, P.G.; Scholtissek, M.; Maier, G. MP2 and DFT Calculations on Circulenes and an Attempt to Prepare the Second Lowest Benzolog, [4]Circulene. *Chem. Eur. J.* **2008**, *14*, 5604–5616. [[CrossRef](#)] [[PubMed](#)]
100. Fabian, J.; Hartmann, H. Structure and Properties of α -Cyclo[N]Thiophenes as Potential Electronic Materials—A Theoretical Study. *J. Phys. Org. Chem.* **2007**, *20*, 554–567. [[CrossRef](#)]
101. Hirshfeld, F.L. Bonded-Atom Fragments for Describing Molecular Charge Densities. *Theor. Chim. Acta* **1977**, *44*, 129–138. [[CrossRef](#)]

102. Fonseca Guerra, C.; Handgraaf, J.-W.; Baerends, E.J.; Bickelhaupt, F.M. Voronoi Deformation Density (VDD) Charges: Assessment of the Mulliken, Bader, Hirshfeld, Weinhold, and VDD Methods for Charge Analysis. *J. Comput. Chem.* **2004**, *25*, 189–210. [[CrossRef](#)] [[PubMed](#)]
103. Davidson, E.R.; Chakravorty, S. A Test of the Hirshfeld Definition of Atomic Charges and Moments. *Theor. Chim. Acta* **1992**, *83*, 319–330. [[CrossRef](#)]
104. Saha, S.; Roy, R.K.; Ayers, P.W. Are the Hirshfeld and Mulliken Population Analysis Schemes Consistent with Chemical Intuition? *Int. J. Quantum Chem.* **2009**, *109*, 1790–1806. [[CrossRef](#)]